Electronic Supplementary Information (ESI)

Distinguishing the respective determining factors for spectral broadening and concentration quenching in multiple resonance typed TADF emitter systems

Feng Huang,[a] Xiao-Chun Fan,[a] Ying-Chun Cheng,[a] Hao Wu,[a] Yi-Zhong Shi,[a] Jia Yu,[a] Kai Wang,[a,b,*] Chun-Sing Lee[c,*] and Xiao-Hong Zhang[a,b,*]

[a]Institute of Functional Nano & Soft Materials (FUNSOM), Jiangsu Key Laboratory for Carbon-Based Functional Materials & Devices, Joint International Research Laboratory of Carbon-Based Functional Materials and Devices, Soochow University, Suzhou, Jiangsu 215123, P. R. China. Email: wkai@suda.edu.cn; xiaohong_zhang@suda.edu.cn

[b]Jiangsu Key Laboratory of Advanced Negative Carbon Technologies, Soochow University, Suzhou, Jiangsu, 215123, P. R. China.

[c]Center of Super-Diamond and Advanced Films (COSDAF) and Department of Chemistry, City University of Hong Kong, Hong Kong SAR, P. R. China. Email: apcslee@cityu.edu.hk

Content

General Information

1. Materials. All commercially available reagents were used as received unless otherwise stated. All reactions were carried out using Schlenk techniques under a nitrogen atmosphere. ^{1}H and ^{13}C NMR spectra were measured on a Bruker 400 MHz spectrometer with tetramethylsilane (TMS) as the internal standard. Mass analyses were recorded by an Autoflex MALDI-TOF mass spectrometer. Elemental analyses (EA) were conducted on a Thermo-FINNI-GAN Flash EA 1112 CHNS/O analyzer.

2. Theoretical calculation. The optimized structure was determined by using Gaussian 09 with a B3LYP/6-31g (d) basis set, and natural transition orbitals (NTOs) of the lowest adiabatic excited states were analyzed via a multifunctional wavefunction analyzer (Multiwfn 3.6).

3. Thermal and electrochemical measurements. Thermogravimetric analysis (TGA) curve was carried on a Perkin Elmer at a heating rate of 10 °C·min^{-1} from 30 to 700 °C under nitrogen. The temperature of 5% weight loss was defined as the decomposition temperature (T_d). Differential scanning calorimetry (DSC) curve was carried on a TA DSC 2010 unit at a heating rate of 10 °C·min^{-1} from 0 to 300 °C under nitrogen. Cyclic voltammetry was performed on a CHI 660 instrument. Individual samples were dissolved in *N,N*-dimethylformamide and degassed with nitrogen gas for 15 minutes before the test. M tetrabutylammonium hexafluorophosphate ($[nBu_4N]PF_6$) acts as the supporting electrolyte, while gold, platinum and a 3.0 M $Ag/AgNO_3$ electrodes play the role of working, counter and reference electrodes, respectively. Cyclic voltammograms (CVs) were obtained at a scan rate of 0.05 V·s^{-1} with standardized against ferrocene/ferrocenium.

4. Measurement of absorption and emission characteristics. UV–Vis absorption spectra were recorded on a Hitachi U-3900 spectrophotometer. PL spectra were recorded on a Hitachi F-4600 fluorescence spectrophotometer with default collection intervals. Transient fluorescence decays were measured with a Quantaurus-Tau fluorescence lifetime spectrometer (C11367-32, Hamamatsu Photonics) with an excitation wavelength of 373 nm and pulse width of 100 ps. The absolute PL quantum yields were recorded on a Hamamatsu Quantaurus-QY quantum yield spectrometer (C13534-11).

5. Single-Crystal Structure. Diffraction data were collected on a Rigaku R-AXIS-RAPID diffractometer using ω-scan mode with graphite-monochromator MoKα radiation. The structure determination was solved with direct methods using the SHELXTL programs and refined with full-matrix least squares on F^2. All crystallographic information in CIF format have been deposited at the Cambridge Crystallographic Center (CCDC) under deposition number 2153530 for TCzBN-DPF and 2161232 for TCzBN-TMPh via www.ccdc.cam.ac.uk/data_request/cif.

6. Device fabrication and measurement of EL characteristics. Before device fabrication, the ITO glass substrates were precleaned carefully. Then, the sample was transferred to the deposition system. The devices were prepared in vacuum at a pressure of 4×10−5 Torr. The hole transporting material TAPC and

TCTA, electron-transporting material TmPyPb, and host material SF_3TRZ were thermally evaporated at a rate of 1.0 $A\omega s^{-1}$. After organic film deposition, 1 nm of LiF and 100 nm of aluminum were thermally evaporated onto the organic surface. The electrical characteristics, electroluminescence spectra, and luminance of the devices were characterized with a Spectra Scan PR 655 PHOTOMETER and a KEITHLEY 2400 Source Meter constant current source at room temperature.

Synthesis

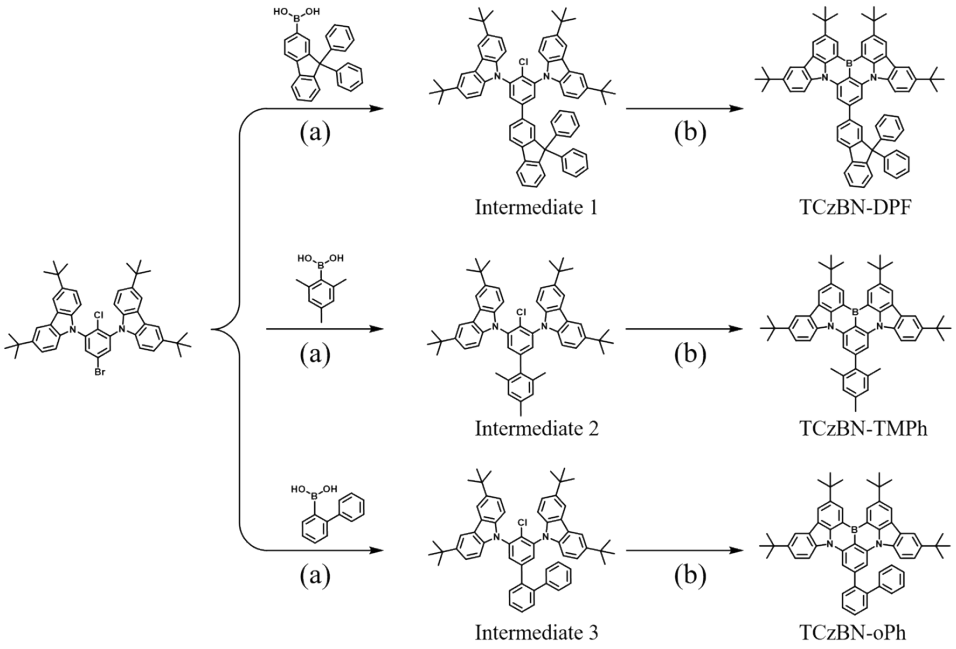

Scheme S1. Synthetic routes for DtBuCzB derivatives. (a) $Pd(PPh_3)_4$, K_2CO_3, Dioxane; (b) 1. t-BuLi, t-BuPh, -50 °C, then 60 °C, 2 h; 2. BBr_3, -40 °C, 1 h, then RT, 1 h; 3. $NEt(i\text{-}Pr)_2$, 0 °C, then 120 °C, 5 h.

Synthesis of **DtBuCzB**: The synthesis process was performed according to the reported literature.[1]

Synthesis of 9,9′-(2-chloro-5-(9,9-diphenyl-9H-fluoren-2-yl)-1,3-phenylene)bis(3,6-di-tert-butyl-9H-carbazole) (**Intermediate 1**): A mixture of 9,9′-(5-bromo-2-chloro-1,3-phenylene)bis(3,6-di-tert-butyl-9H-carbazole) (3.73 g, 5.0 mmol), (9,9-diphenyl-9H-fluoren-2-yl)boronic acid (2.71 g, 7.5 mmol), $Pd(PPh_3)_4$ (115.56 mg, 0.1 mmol), 2.0 M potassium carbonate aqueous solution (5 mL, 10 mmol) and 50 mL dioxane were added to a 250 mL two-neck flask and refluxed at 110 °C under N_2 protection for 12 hours. After the reaction was cooled to room temperature, the mixture was extracted with dichloromethane and water three times to collect the organic layer. Then, the collection was dried with $MgSO_4$ and concentrated with rotary evaporation. The residue was purified via column chromatography eluting with petroleum ether: dichloromethane (10:1) to obtain a white solid (4.10 g, yield: 83%).

Synthesis of 9,9′-(4-chloro-2′,4′,6′-trimethyl-[1,1′-biphenyl]-3,5-diyl)bis(3,6-di-tert-butyl-9H-carbazole) (**Intermediate 2**): Intermediate 2 was synthesized according to the same procedure as for

intermediate 1 by using 2,4,6-trimethylphenylboronic acid (1.23 g, 7.5 mmol) instead (9,9-diphenyl-9H-fluoren-2-yl)boronic acid. White solid (3.49 g, yield: 89%).

Synthesis of 9,9′-(4-chloro-[1,1′:2′,1″-terphenyl]-3,5-diyl)bis(3,6-di-tert-butyl-9H-carbazole) (**Intermediate 3**): Intermediate 3 was synthesized according to the same procedure as for intermediate 1 by using 2-diphenylboronic acid (1.48 g, 7.5 mmol) instead (9,9-diphenyl-9H-fluoren-2-yl)boronic acid. White solid (3.44 g, yield: 84%).

Synthesis of **TCzBN-DPF**: Intermediate 1 (4.92 g, 5.0 mmol) and tert-butylbenzene (60 mL) were added to a dried 250 mL two-neck flask in a nitrogen atmosphere. After stirring for dissolution, a solution of tert-butyllithium in pentane (6.2 mL, 1.60 M, 10.0 mmol) was added slowly to the solution at -50 °C. Then, the mixture was heated to 60 °C and stirred for 2 hours. After the removal of pentane in vacuo, boron tribromide (1.0 mL, 10.0 mmol) was injected slowly into the reaction at -50 °C. The reaction was warmed to room temperature, and the mixture was stirred for 1 hour. Then, N,N-diisopropylethylamine (1.7 mL, 10.0 mmol) was added at 0 °C, and the reaction was stirred at 130 °C for another 5 hours. After the reaction was cooled to room temperature, a phosphorus buffer solution (pH 6, 10 mL) was added, and the aqueous layer was separated and extracted with dichloromethane and water. The collected organic layer was dried with $MgSO_4$ and concentrated in vacuo to give the crude product. Furthermore, the crude product was purified via column chromatography eluting with petroleum ether: dichloromethane (10:1) to obtain a yellow solid (1.62 g, yield: 34%). ^{1}H NMR (400 MHz, Chloroform-*d*) δ 9.15 (d, J = 1.9 Hz, 2H), 8.53 – 8.48 (m, 4H), 8.36 (d, J = 8.8 Hz, 2H), 8.30 (d, J = 2.0 Hz, 2H), 8.07 – 7.91 (m, 4H), 7.66 (dd, J = 8.8, 2.1 Hz, 2H), 7.57 (dd, J = 7.6, 1.0 Hz, 1H), 7.48 (td, J = 7.4, 1.1 Hz, 1H), 7.43 – 7.30 (m, 11H), 1.70 (s, 18H), 1.58 (s, 18H). ^{13}C NMR (101 MHz, $CDCl_3$) δ 152.28, 151.48, 146.04, 145.30, 144.69, 141.75, 141.35, 140.40, 139.84, 138.31, 129.83, 128.43, 128.31, 128.10, 127.75, 127.35, 127.17, 126.77, 126.40, 126.02, 124.46, 123.62, 120.80, 120.65, 120.55, 117.30, 114.19, 107.08, 65.72, 35.18, 34.80, 32.20, 31.85. MALDI-TOF MS (mass m/z): 956.5241 $[M]^+$; calcd for $C_{71}H_{65}BN_2$ 956.9584. Anal. Calcd (%) for C, 89.10; H, 6.85; B, 1.13; N, 2.93; Found: C, 88.96; H, 6.93; N, 2.86.

Synthesis of **TCzBN-TMPh**: TCzBN-TMPh was synthesized according to the same procedure as for TCzBN-DPF by using Intermediate 3 (3.93 g, 5.0 mmol) instead of Intermediate 1 (4.92 g, 5.0 mmol). TCzBN-oPh (1.32 g, yield: 35%) was obtained as a yellow solid. ^{1}H NMR (400 MHz, Chloroform-*d*) δ 9.19 (d, *J* = 1.7 Hz, 2H), 8.51 (d, *J* = 1.7 Hz, 2H), 8.34 – 8.27 (m, 4H), 8.17 (s, 2H), 7.60 (dd, *J* = 8.8, 2.0 Hz, 2H), 7.14 (s, 2H), 2.48 (s, 3H), 2.26 (s, 6H), 1.72 (s, 18H), 1.54 (s, 18H). ^{13}C NMR (101 MHz, $CDCl_3$) δ 146.51, 145.34, 144.70, 144.50, 141.70, 139.57, 138.28, 137.22, 136.12, 129.85, 128.31, 127.03, 124.35, 123.64, 120.65, 117.19, 114.26, 109.05, 35.20, 34.77, 32.22, 31.81, 21.19, 20.89. MALDI-TOF MS (mass m/z): 758.8832 $[M]^+$; calcd for $C_{55}H_{59}BN_2$ 758.4771. Anal. Calcd (%) for C, 87.05; H, 7.84; B, 1.42; N, 3.69; Found: C, 87.15; H, 7.75; N, 3.57.

Synthesis of **TCzBN-oPh**: TCzBN-oPh was synthesized according to the same procedure as for TCzBN-DPF by using Intermediate 2 (4.10 g, 5.0 mmol) instead of Intermediate 1 (4.92 g, 5.0 mmol).

TCzBN-oPh (1.51 g, yield: 38%) was obtained as a yellow solid. ^{1}H NMR (400 MHz, Chloroform-*d*) δ 9.13 (d, J = 1.7 Hz, 2H), 8.47 (d, J = 1.7 Hz, 2H), 8.25 (d, J = 1.9 Hz, 2H), 8.17 (s, 2H), 7.80 – 7.77 (m, 1H), 7.73 – 7.67 (m, 3H), 7.64 – 7.50 (m, 6H), 7.36 (t, J = 7.7 Hz, 2H), 7.21 (t, J = 7.4 Hz, 1H), 1.69 (s, 18H), 1.55 (s, 18H). ^{13}C NMR (101 MHz, $CDCl_3$) δ 146.28, 145.19, 144.60, 143.79, 141.65, 141.41, 140.83, 138.18, 131.31, 131.19, 130.23, 129.71, 128.34, 127.96, 127.19, 126.84, 124.15, 123.60, 120.59, 117.07, 114.07, 110.31, 35.17, 34.76, 32.20, 32.00, 31.83. MALDI-TOF MS (mass m/z): 792.8493 $[M]^+$; calcd for $C_{58}H_{57}BN_2$ 792.4615. Anal. Calcd (%) for C, 87.86; H, 7.25; B, 1.36; N, 3.53; Found: C, 87.77; H, 7.36; N, 3.44.

Theoretical Calculations

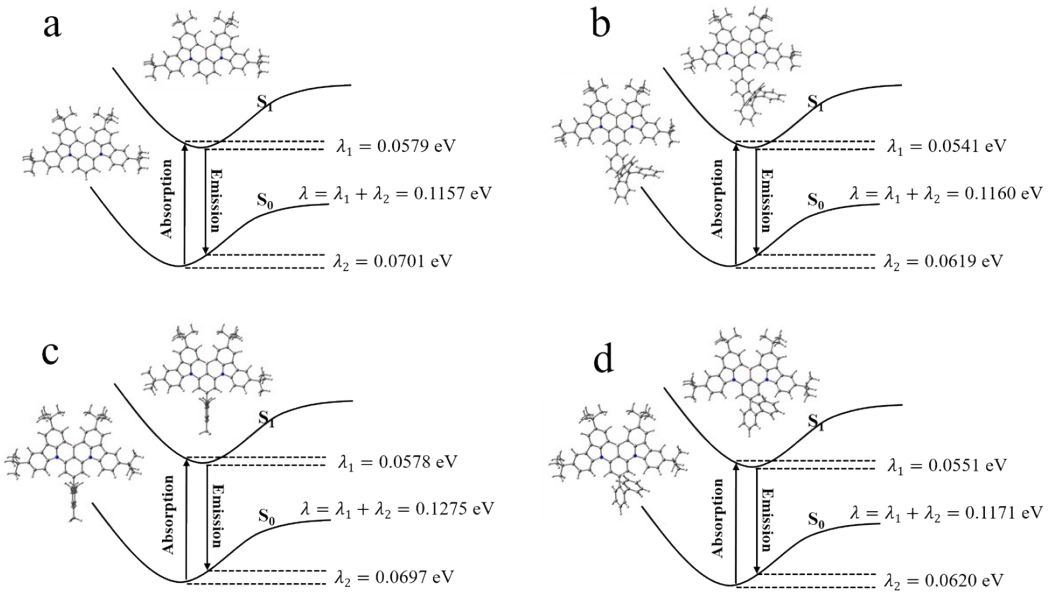

Figure S1. Reorganization energies with optimized S_0 and S_1 geometries and single point energies of (a) DtBuCzB, (b) TCzBN-DPF, (c) TCzBN-TMPh and (d) TCzBN-oPh.

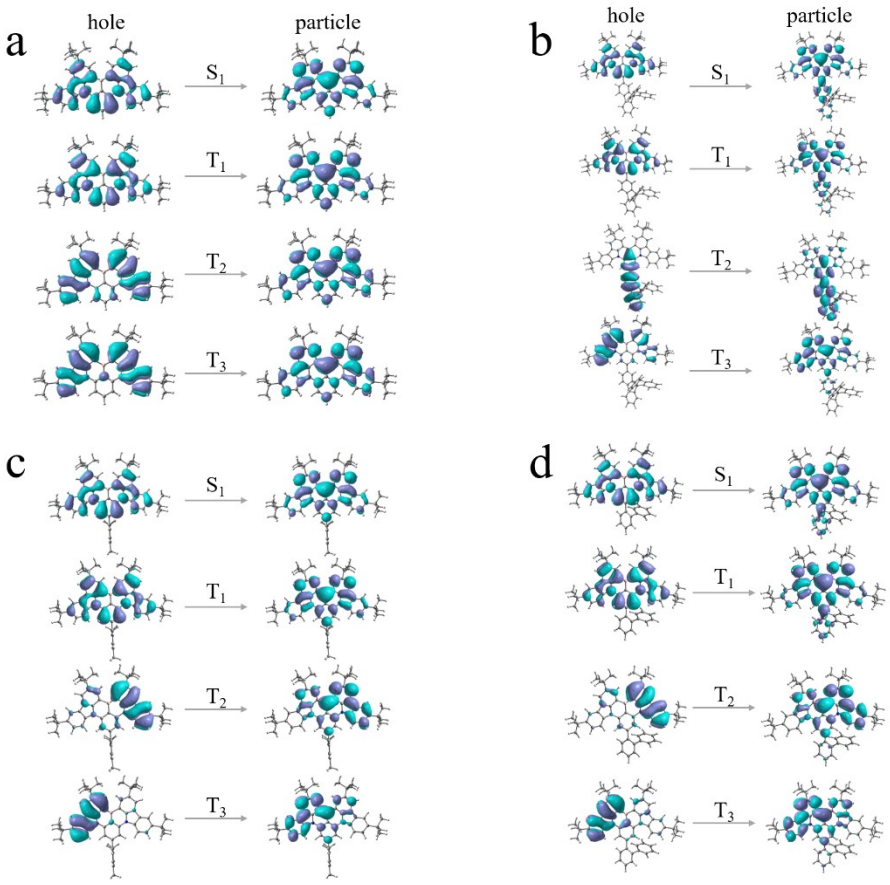

Figure S2. Calculated natural transition orbital (NTO) distributions of (a) DtBuCzB, (b) TCzBN-DPF, (c) TCzBN-TMPh and (d) TCzBN-oPh in their excited states.

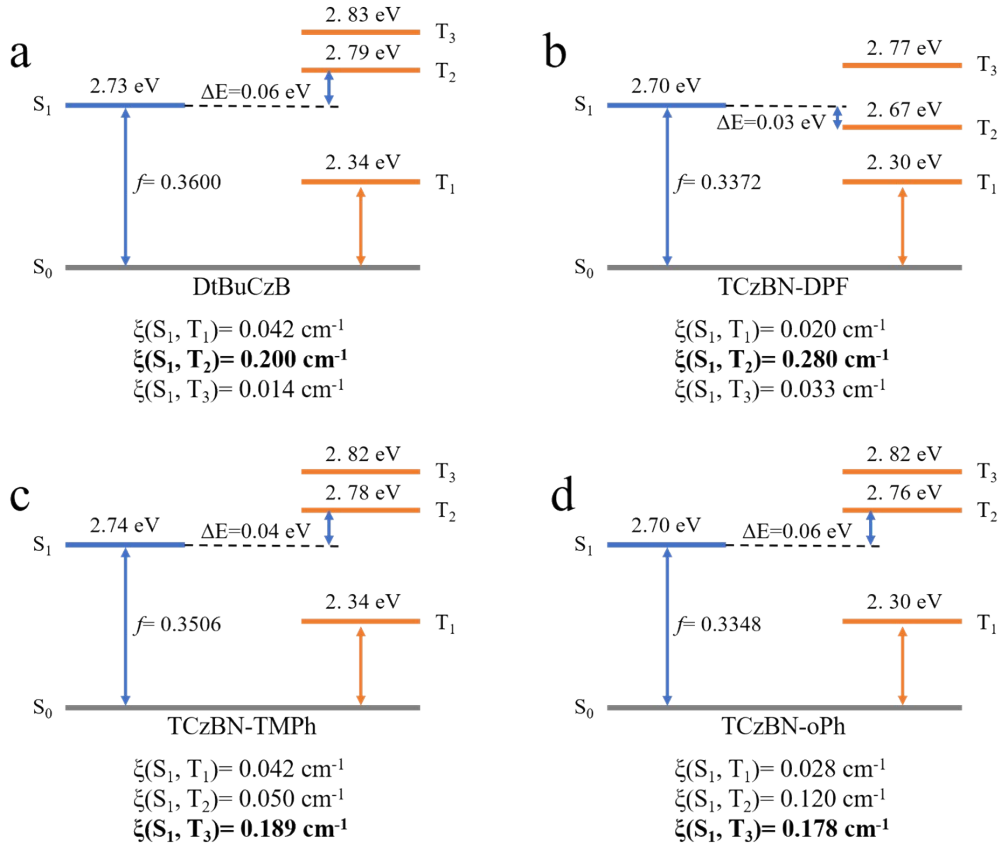

Figure S3. Theoretically estimated energy diagrams of (a) DtBuCzB, (b) TCzBN-DPF, (c) TCzBN-TMPh and (d) TCzBN-oPh and their SOC matrix elements between the T_n (n=1, 2, 3) and S_1 states.

Thermal and electrochemical measurements

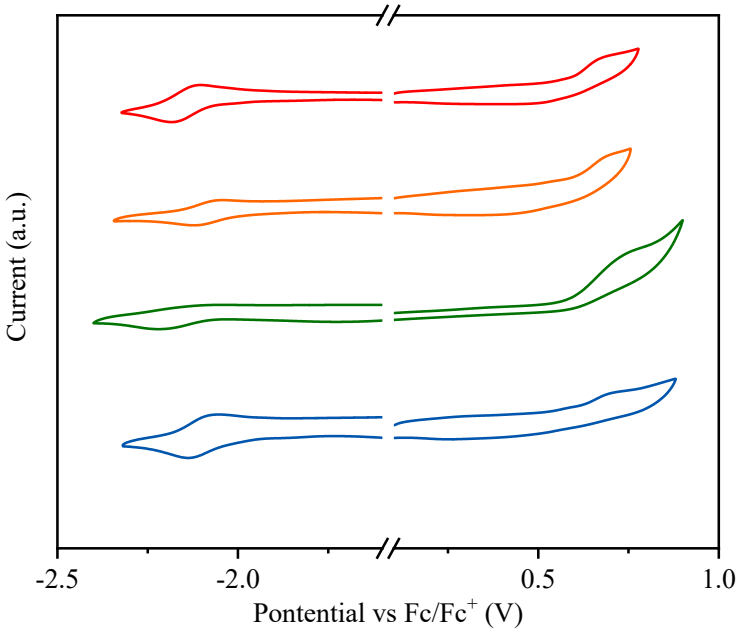

Figure S4. Cyclic voltammogram (CV) curves of DtBuCzB (red), TCzBN-DPF (orange), TCzBN-TMPh (green) and TCzBN-oPh (blue) in degassed DMF solutions.

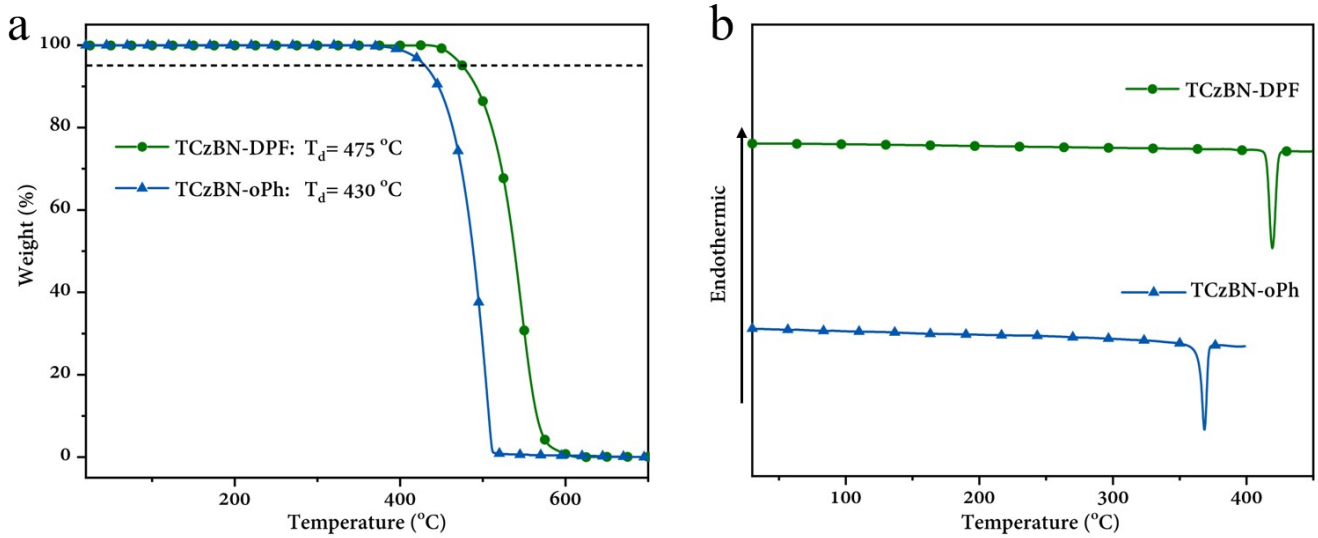

Figure S5. TGA traces (a) and DSC traces (b) of TCzBN-DPF and TCzBN-oPh.

Photophysical Properties

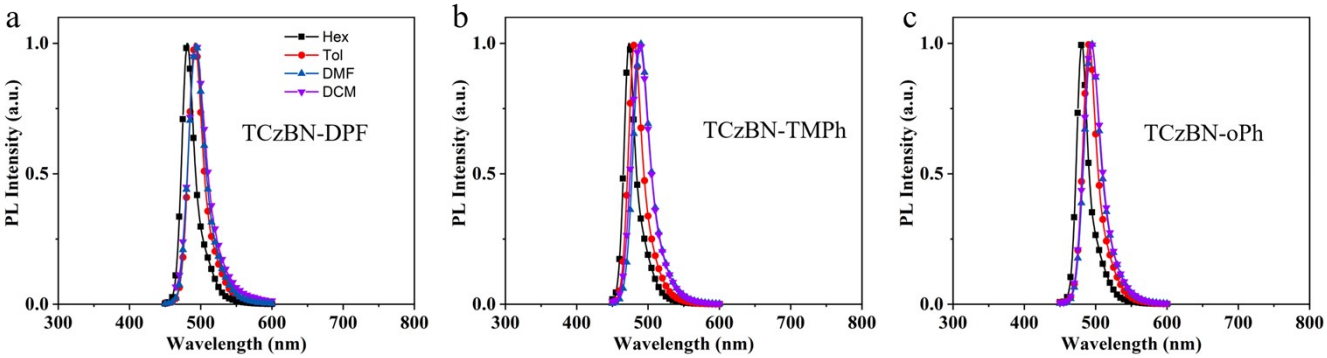

Figure S6. Fluorescence spectra of (a) TCzBN-DPF, (b) TCzBN-TMPh and (c) TCzBN-oPh in different solvents.

Table S1. Summary of the fluorescence and phosphorescence wavelengths and corresponding energy levels of the MR emitters at 77 K.

Emitters	wt [%]	FL [nm]	PL [nm]	S_1 [eV]	T_1 [eV]	ΔE_{ST} [eV]
DtBuCzB	1	493	514	2.51	2.41	0.10
	5	498	519	2.49	2.39	0.10
	10	503	525	2.47	2.36	0.11
	20	507	534	2.44	2.32	0.12
TCzBN-DPF	1	499	520	2.48	2.38	0.10
	5	503	524	2.46	2.36	0.10
	10	506	528	2.45	2.34	0.11
	20	508	536	2.44	2.31	0.13
TCzBN-TMPh	1	491	511	2.52	2.42	0.10
	5	494	517	2.51	2.40	0.11
	10	495	520	2.50	2.38	0.12
	20	496	526	2.50	2.36	0.14
TCzBN-oPh	1	495	516	2.50	2.40	0.10
	5	500	520	2.48	2.38	0.10
	10	502	526	2.47	2.35	0.12
	20	505	533	2.45	2.32	0.13

Kinetic Analysis

The key kinetic parameters of the MR emitters are estimated according to the following equations, and the key kinetic parameters are summarized in Table S2.

$$PLQY = \varphi_p + \varphi_d$$

$$k_p = \frac{1}{\tau_p}$$

$$k_d = \frac{1}{\tau_d}$$

$$k_r^S = k_p \varphi_p$$

$$k_{ISC} = k_p(1 - \varphi_p)$$

$$k_{RISC} = \frac{k_p k_d \varphi_d}{k_{ISC} \varphi_p}$$

$$k_{CQ} = \frac{1}{2}(k_p + k_d - 2k_{RISC} - \sqrt{(k_p - k_d)^2 - 4k_{ISC}k_{RISC}})$$

where φ_p and φ_d are the prompt and delayed fluorescence quantum efficiencies, respectively;

k_r^S are the rate constants of the singlet radiative transition;

k_p, k_d, k_{ISC} and k_{RISC} are the rate constants of prompt fluorescence, delayed fluorescence decay, ISC and RISC processes, respectively;

k_{CQ} are the rate constants of the concentration quenching process.[2-4]

Table S2. Calculated dynamic parameters of MR emitters in SF_3TRZ films with different doping concentrations from 1 wt% to 20 wt%.

Emitters	wt (%)	PLQY (%)	φ_p (%)	φ_d (%)	τ_p [ns]	τ_d [μs]	k_p (10^8 s^{-1})	k_r^s (10^8 s^{-1})	k_d (10^3 s^{-1})	k_{ISC} (10^8 s^{-1})	k_{RISC} (10^4 s^{-1})	k_{CQ} (10^3 s^{-1})
DtBuCzB	1	92.9	50.2	42.7	6.1	127	1.65	0.83	7.86	0.82	1.34	1.12
	5	85.9	59.7	26.2	4.4	123	2.27	1.36	8.09	0.91	0.88	2.84
	10	77.0	52.3	24.7	3.9	118	2.59	1.36	8.42	1.24	0.83	4.06
	20	69.5	57.6	11.9	3.7	96	2.69	1.55	10.4	1.14	0.51	7.45
TCzBN-DPF	1	96.9	43.8	53.1	5.7	55	1.82	0.77	18.2	0.99	3.92	1.01
	5	96.1	47.7	48.4	5.3	56	1.78	0.90	17.8	0.98	3.45	1.33
	10	95.7	53.6	42.1	5.7	56	1.78	0.93	17.8	0.81	3.01	1.65
	20	92.1	59.0	33.1	4.4	55	1.81	1.33	18.1	0.92	2.48	3.49
TCzBN-TMPh	1	94	46.1	47.9	5.8	105	1.73	0.80	9.48	0.93	1.83	1.06
	5	89.8	50.0	39.8	4.6	97	2.18	1.09	10.3	1.09	1.63	2.09
	10	82.4	53.0	29.4	3.9	92	2.57	1.37	10.8	1.21	1.27	4.05
	20	74.0	59.3	14.7	2.5	92	4.07	2.41	10.8	1.66	0.66	6.87
TCzBN-oPh	1	96.1	50.6	45.5	5.9	112	1.71	0.86	8.91	0.84	1.62	0.71
	5	95.7	58.4	37.3	5.2	111	1.92	1.12	8.99	0.80	1.38	0.93
	10	92.1	66.6	25.5	4.0	104	2.48	1.65	9.60	0.83	1.10	2.27
	20	86.0	61.6	24.4	3.8	102	2.64	1.63	9.78	1.01	1.01	3.57

Table S3. Calculated intermolecular distance of the MR emitters in doped films.

	Intermolecular distance (nm)[a]			
	1 wt%	5 wt%	10 wt%	20 wt%
DtBuCzB	4.34	2.54	2.02	1.60
TCzBN-DPF	4.96	2.90	2.30	1.83
TCzBN-TMPh	4.59	2.69	2.13	1.69
TCzBN-oPh	4.66	2.73	2.16	1.72

[a]The intermolecular distance (R) is calculated via $R = [\rho \times \beta \times \frac{N_A}{M_g}]^{-\frac{1}{3}}$, where ρ is the film density ($\approx 1.3\ g\ cm^{-3}$), β is the dopant concentration in the film (wt%), N_A is the Avogadro number and M_g is the dopant molecular weight.[5]

Crystallographic Data

Table S4. Crystal data and structure refinement for TCzBN-DPF and TCzBN-TMPh.

Empirical formula	$C_{71}H_{65}BN_2$
Formula weight	957.06
Temperature/K	150
Crystal system	triclinic
Space group	P -1
Hall group	-P 1
a/Å	15.3343 (7)
b/Å	16.0574 (7)
c/Å	17.7726 (7)
α/°	93.9950 (10)
β/°	113.8040 (10)
γ/°	110.9540 (10)
Volume/Å^3	3619.9 (3)
Z	2

Density	0.878
μ/mm^{-1}	0.050
F(000)	1020
θ range/Å	2.304-26.166
Crystal size/mm^3	0.15ᔓ0.08ᔓ0.05
Radiation	Mokα (λ = 0.71073)
Index ranges	-19 ≤ h ≤ 18, -18 ≤ k ≤ 20, -22 ≤ l ≤ 22
Reflections collected	41304
R (reflections)	0.0671 (7153)
*w*R2 (reflections)	0.1981 (14691)

Empirical formula	$C_{55}H_{59}BN_2$
Formula weight	758.85
Temperature/K	150
Crystal system	monoclinic
Space group	P 1 21/c 1
Hall group	-p 2ybc
a/Å	12.0821 (7)
b/Å	31.477 (2)
c/Å	11.6968 (8)
α/°	90
β/°	98.973 (2)
γ/°	90
Volume/ Å^3	4397.0 (5)
Z	4
Density	1.147
μ/mm^{-1}	0.065
F(000)	1632.0
θ range/Å	2.898-26.363
Crystal size/mm^3	0.15ᔓ0.08ᔓ0.05
Radiation	Mokα (λ = 0.71073)
Index ranges	-15 ≤ h ≤ 13, -39 ≤ k ≤ 34, -13 ≤ l ≤ 14
Reflections collected	27185
R(reflections)	0.0692 (4353)
*w*R2(reflections)	0.1806 (8735)

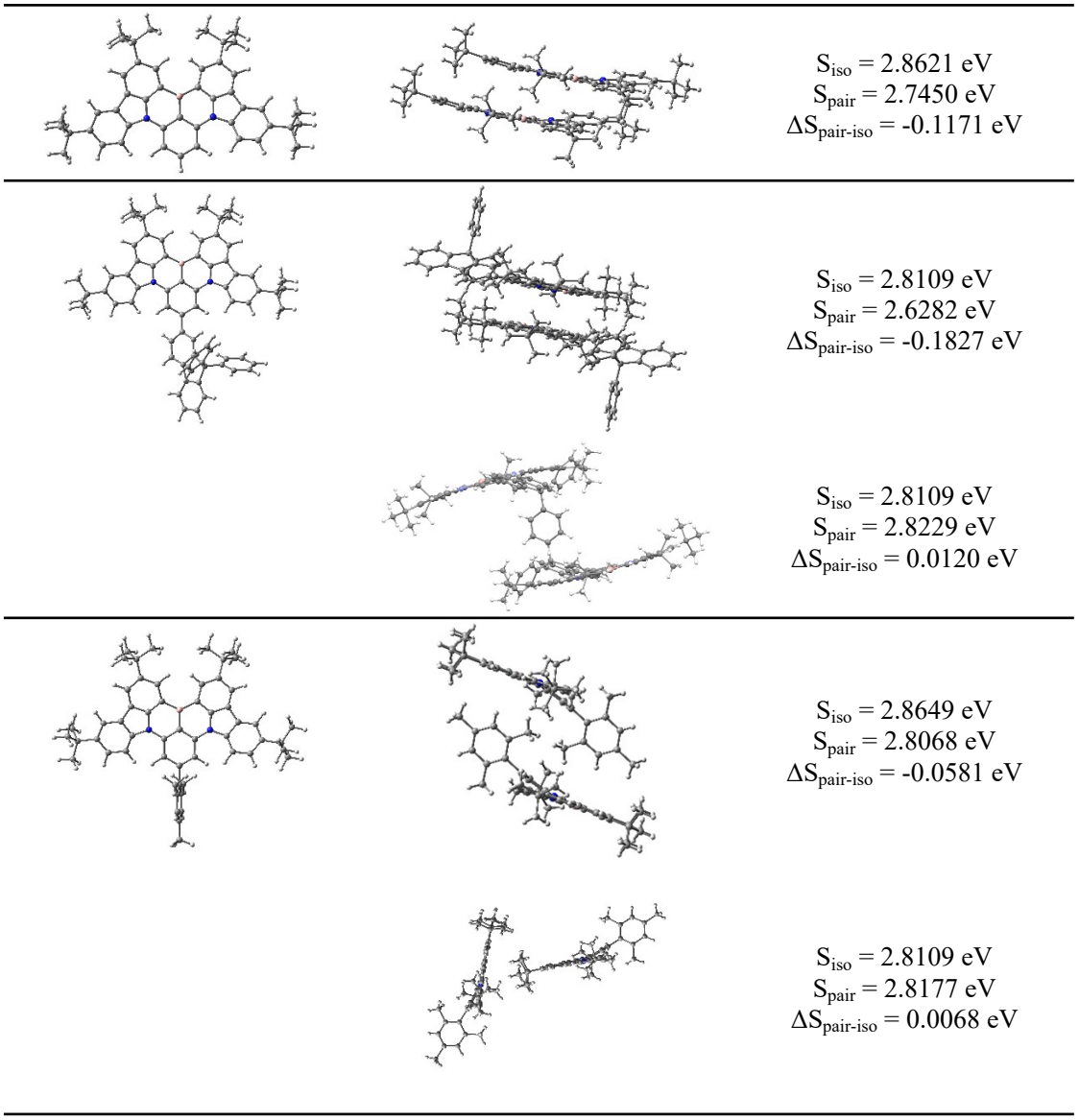

Figure S7. Calculation of the S_1 energy level of isolated molecules and molecule pairs for DtBuCzB, TCzBN-DPF and TCzBN-TMPh according to their stacking modes in crystal.

Device Characterization

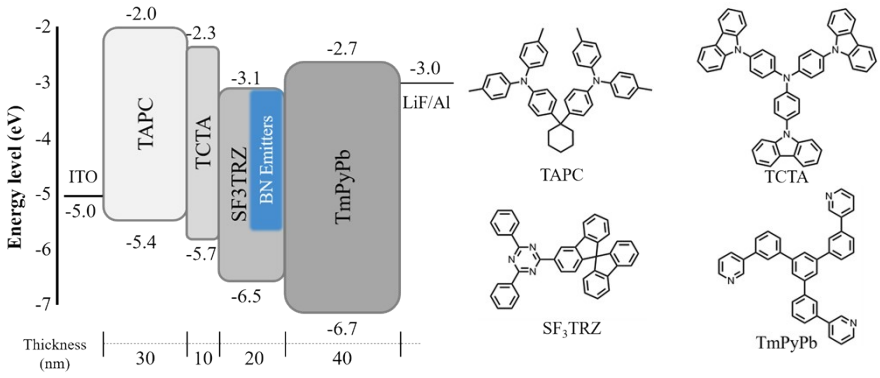

Figure S8. Device architecture for MR BN system emitters with energy level alignment and materials utilized in device fabrication.

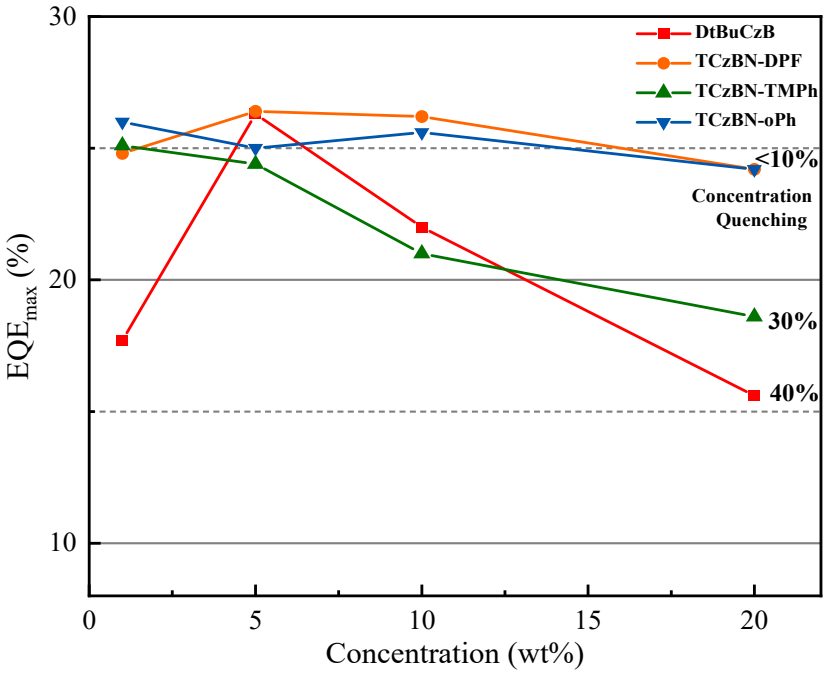

Figure S9. Maximum external quantum efficiency-concentration relationship of the OLEDs based on DtBuCzB (red), TCzBN-DPF (orange), TCzBN-oPh (green) and TCzBN-TMPh (blue).

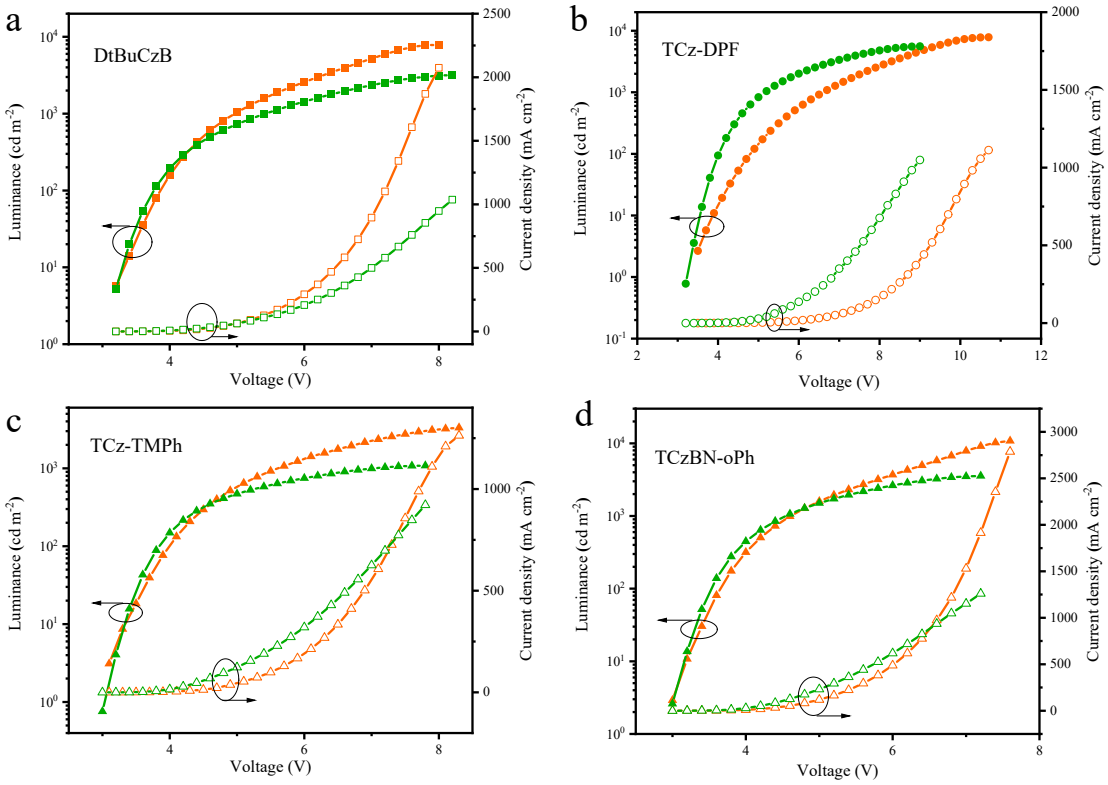

Figure S10. Luminance-voltage-current density characteristics of the OLEDs based on (a) DtBuCzB, (b) TCzBN-DPF, (c) TCzBN-TMPh and (d) TCzBN-oPh at 5 wt% (orange line) and 20 wt% (green line) doping concentrations.

Table S5. Summary of the OLED performances based on these MR emitters.

Emitters	Concentration [wt%]	λ_{max}[a] [nm]	FWHM[b] [nm/eV]	EQE[c] [%]	CIE[d] (x, y)
DtBuCzB	1	488	28/0.145	17.7/16.8/8.6	0.09, 0.37
	5	490	31/0.158	26.3/21.1/9.0	0.10, 0.45
	10	492	37/0.186	22.0/16.4/3.9	0.12, 0.50
	20	493	43/0.212	15.6/12.2/3.4	0.14, 0.54
TCzBN-DPF	1	496	28/0.140	24.8/19.1/11.3	0.09, 0.53

	5	498	31/0.156	26.4/22.8/12.0	0.10, 0.56
	10	500	32/0.158	26.2/23.7/12.9	0.12, 0.58
	20	501	36/0.175	24.2/19.2/9.2	0.17, 0.60
TCzBN-TMPh	1	488	27/0.140	25.1/18.4/6.5	0.11, 0.38
	5	488	27/0.139	24.4/18.3/5.2	0.09, 0.37
	10	488	27/0.139	21.0/17.8/4.7	0.10, 0.39
	20	488	27/0.139	18.6/6.9/0.8	0.10, 0.39
TCzBN-oPh	1	492	28/0.142	26.0/22.9/10.4	0.09, 0.46
	5	495	29/0.146	25.0/20.8/8.4	0.09, 0.51
	10	496	29/0.145	25.6/21.2/6.4	0.10, 0.52
	20	496	31/0.154	24.2/14.7/3.7	0.11, 0.54

[a]Maximum electroluminescence wavelength. [b]Full width at half maximum of electroluminescence. [c]Maximum efficiency/efficiency at 100 cd$\cdot$m^{-2}/efficiency at 1000 cd$\cdot$m^{-2}. [d]Recorded at 10 cd$\cdot$m^{-2}.

NMR Spectra

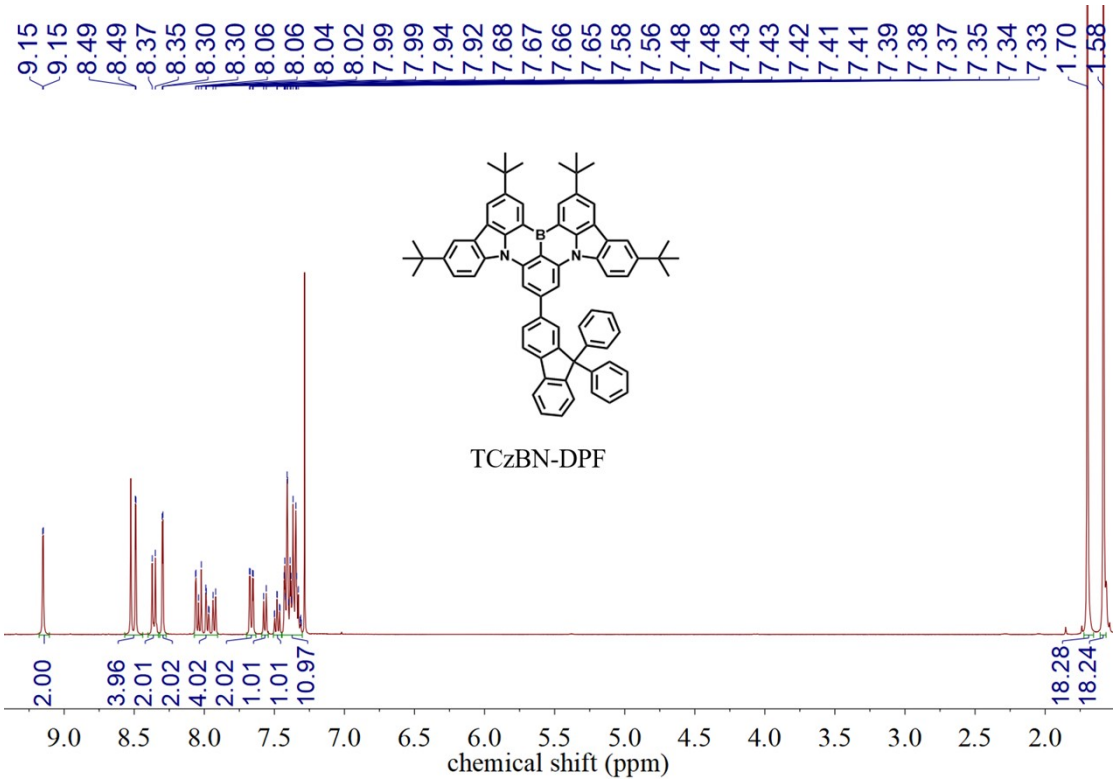

Figure S11. [1]H NMR spectrum of TCzBN-DPF in Chloroform-*d*.

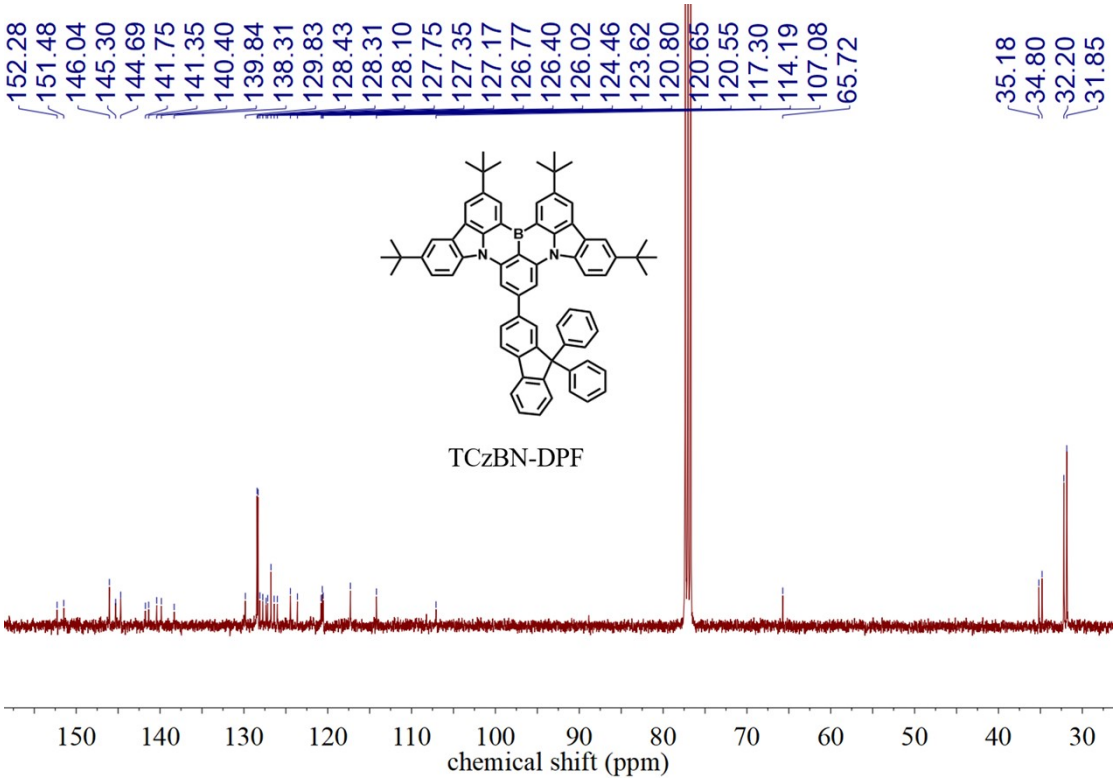

Figure S12. ^{13}C NMR spectrum of TCzBN-DPF in Chloroform-*d*.

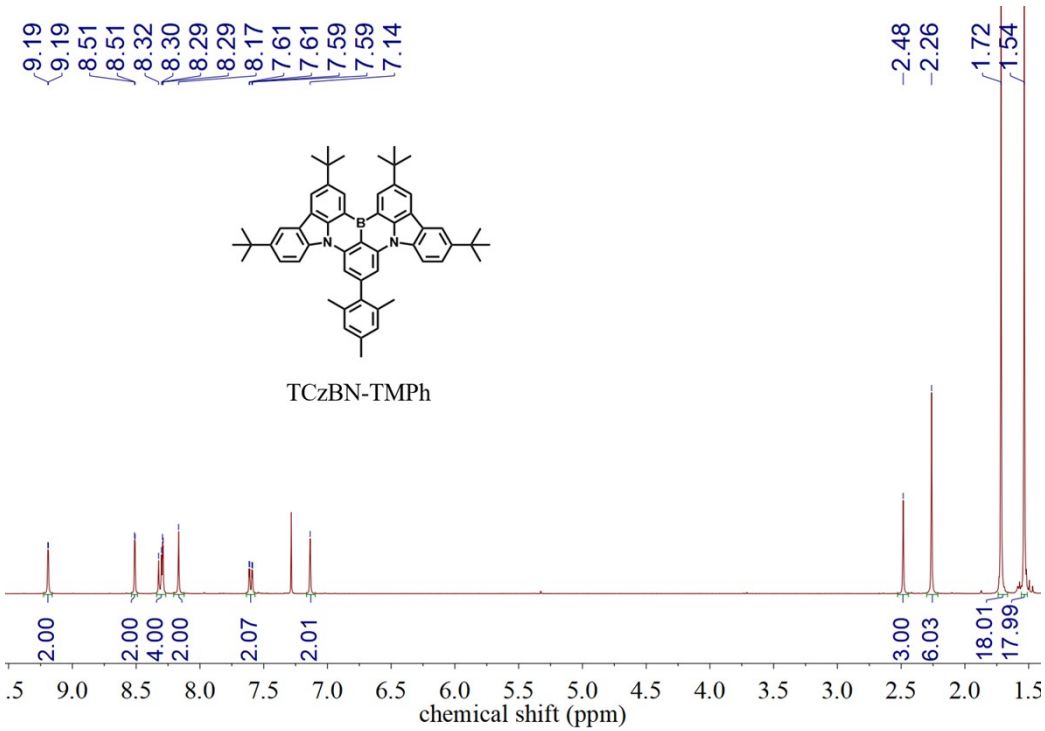

Figure S13. ^{1}H NMR spectrum of TCzBN-TMPh in Chloroform-*d*.

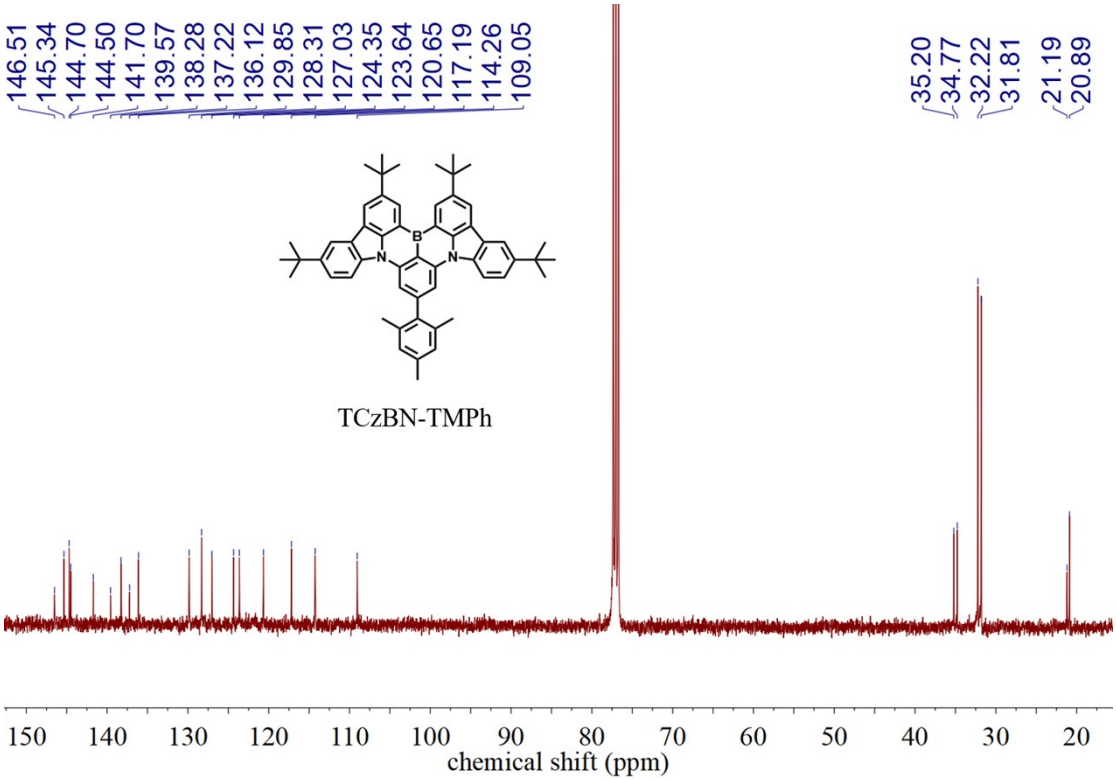

Figure S14. ^{13}C NMR spectrum of TCzBN-TMPh in Chloroform-*d*.

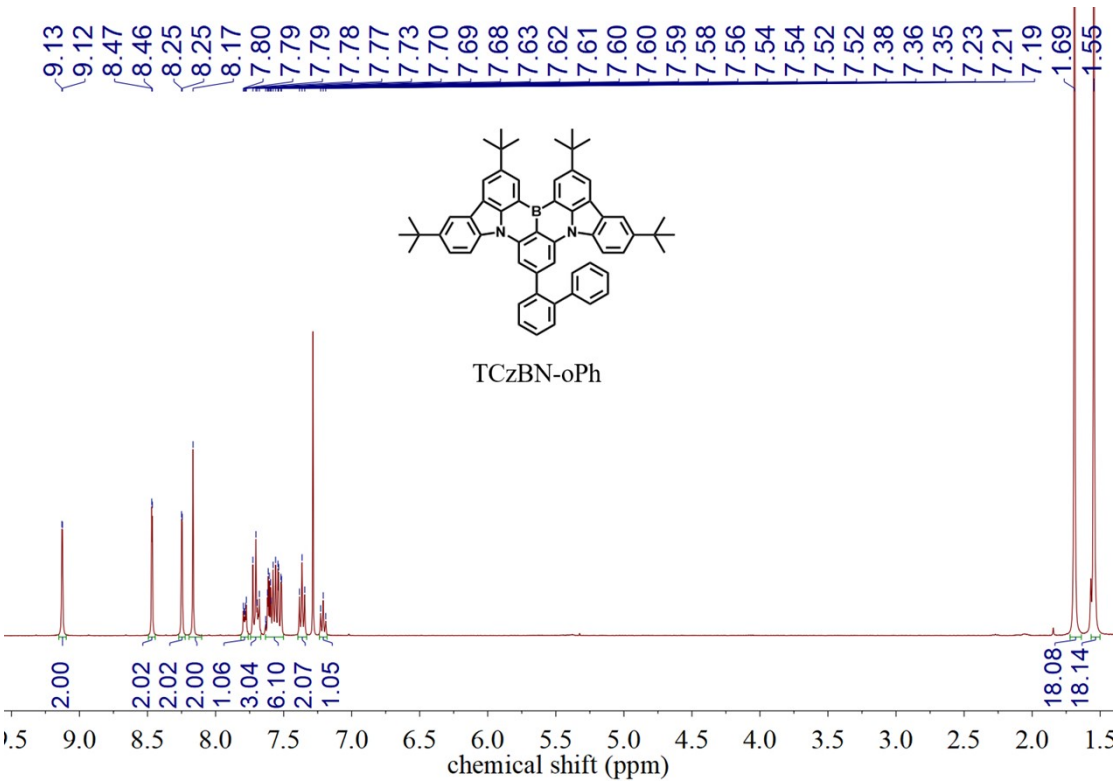

Figure S15. ^{1}H NMR spectrum of TCzBN-oPh in Chloroform-*d*.

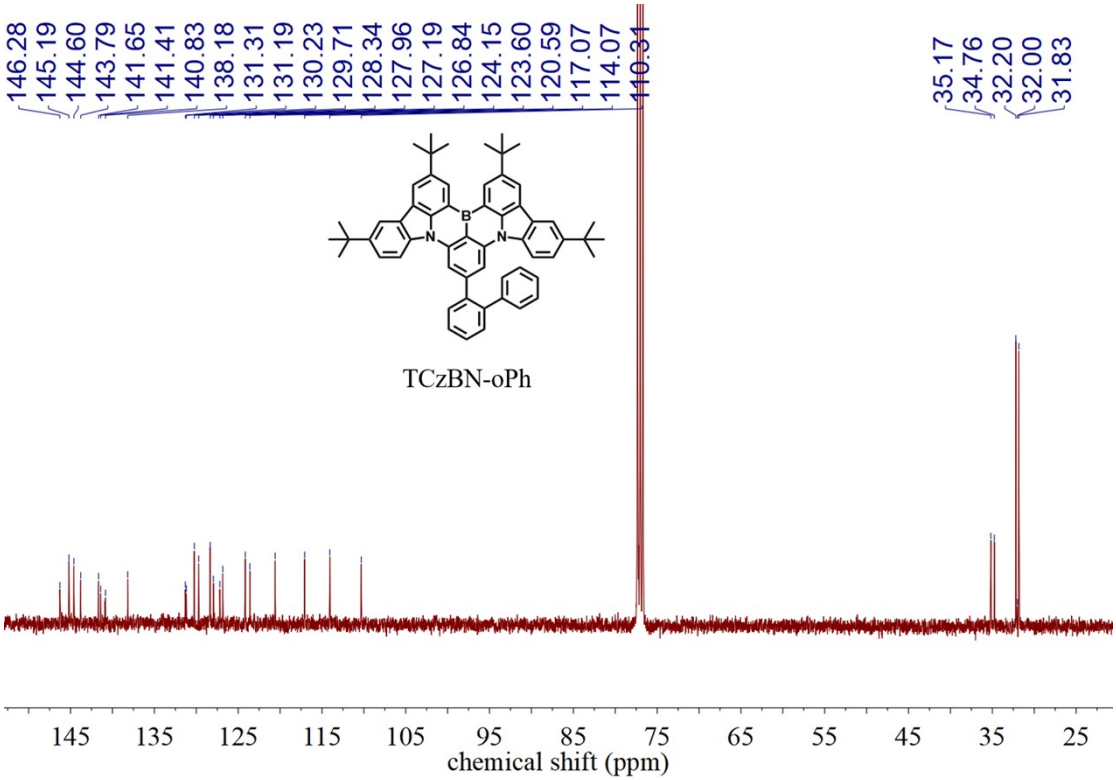

Figure S16. ^{13}C NMR spectrum of TCzBN-oPh in Chloroform-*d*.

References

1. Y. Xu, Z. Cheng, Z. Li, B. Liang, J. Wang, J. Wei, Z. Zhang, Y. Wang, *Adv. Opt. Mater.* 2020, **8**, 1902142.
2. D. Kasemann, R. Brückner, H. Fröb, K. Leo, *Phys. Rev. B* 2011, **84**, 115208.
3. Y. Zhang, S. R. Forrest, *Phys. Rev. Lett.* 2012, **108**, 267404.
4. J. Lee, N. Aizawa, M. Numata, C. Adachi, T. Yasuda, *Adv. Mater.* 2017, **29**, 1604856.
5. D. Karthik, Y. H. Jung, H. Lee, S. Hwang, B. M. Seo, J. Y. Kim, C. W. Han, J. H. Kwon, *Adv. Mater.* 2021, **33**, 2007724.